

Future Medicine Ltd

Nanomedicine

Volume 16, Issue 1, January 2021, Pages 37-50

<https://doi.org/10.2217/nnm-2020-0263>

Open Access



Nanomedicine



Research Article

Improved therapeutic antibody delivery to xenograft tumors using cavitation nucleated by gas-entrapping nanoparticles

Megan Grundy¹, Luca Bau¹, Claudia Hill¹, Catherine Paverd¹, Christophoros Mannaris¹, James Kwan², Calum Crane³, Christian Coviello³, Constantin Coussios¹ & Robert Carlisle^{1,*}

¹Department of Engineering Science, Biomedical Ultrasonics, Biotherapy and Biopharmaceuticals Laboratory (BUBBL), Institute of Biomedical Engineering (IBME), University of Oxford, Old Road Campus Research Building, Headington, Oxford OX3 7DQ, UK

²Department of Engineering Science, University of Oxford, Oxford OX1 3PJ, UK

³OxSonics Therapeutics, Oxford Science Park, Oxford OX4 4GA, UK

*Author for correspondence: robert.carlisle@eng.ox.ac.uk

Aims: Testing ultrasound-mediated cavitation for enhanced delivery of the therapeutic antibody cetuximab to tumors in a mouse model. **Methods:** Tumors with strong EGF receptor expression were grown bilaterally. Cetuximab was coadministered intravenously with cavitation nuclei, consisting of either the ultrasound contrast agent Sonovue or gas-stabilizing nanoscale SonoTran Particles. One of the two tumors was exposed to focused ultrasound. Passive acoustic mapping localized and monitored cavitation activity. Both tumors were then excised and cetuximab concentration was quantified. **Results:** Cavitation increased tumoral cetuximab concentration. When nucleated by Sonovue, a 2.1-fold increase (95% CI 1.3- to 3.4-fold) was measured, whereas SonoTran Particles gave a 3.6-fold increase (95% CI 2.3- to 5.8-fold). **Conclusions:** Ultrasound-mediated cavitation, especially when nucleated by nanoscale gas-entrapping particles, can noninvasively increase site-specific delivery of therapeutic antibodies to solid tumors.

First draft submitted: 20 June 2020; **Accepted for publication:** 4 November 2020; **Published online:** 11 January 2021.

Keywords: antibody • cavitation • drug delivery • nanoparticle • PAM • targeted therapy • ultrasound

Currently, approximately 15 therapeutic monoclonal antibodies have been approved for use in the treatment of solid tumors. These antibodies have many advantages over other more traditional chemotherapeutics, particularly in their extended circulation kinetics, target-specificity and variety of mechanisms of action [1]. However, the large size of these macromolecules (~150 kDa) can hinder efficient extravasation and penetration into solid tumors, which are often characterized by high interstitial fluid pressure and reduced

convective flow [2]. Additionally, the “binding-site barrier” – the process whereby antibodies immediately bind with high affinity to the first target ligand they encounter upon entry into the tumor – can prevent extravasation beyond the perivascular space [3]. In animal models, studies using immunohistochemistry have demonstrated heterogeneous tumoral distribution of monoclonal antibodies such as cetuximab and trastuzumab, particularly at low doses of antibody and at early time points postinjection. Even after high dosing and extended circulation time, however, certain tumor regions with confirmed target receptor expression with little to no bound therapeutic antibody were still found [4–6]. Moreover, Baker *et al.* did not find a consistent correlation between regional measures of vascular supply (vascular density, vessel patency, maturity and function) and antibody distribution. This finding, coupled with the observation that similar levels of antibody distribution can be achieved in the presence of varying degrees of receptor expression, indicates that other vessel or tissue barriers (in addition to the binding site barrier and limited perfusion/convection) could limit therapeutic antibody delivery and distribution [6]. Therefore, if treatment of solid tumors with monoclonal antibodies is to achieve optimal therapeutic success, these delivery challenges need to be addressed. Current clinical treatment of solid tumors with antibody monotherapy could be considered suboptimal [7]. A recent clinical study using the anti-EGFR antibody panitumumab demonstrated substantial intra- and inter-tumor and interpatient heterogeneity in the delivery of therapeutic antibody to solid head and neck tumors. Indeed, the authors showed that in some cases, intratumoral distribution of the antibody was restricted to perivascular regions, regardless of high levels of EGFR expression being present throughout the tumor [8].

Focused ultrasound (US) has emerged as a noninvasive and drug-agnostic technique to improve drug delivery in a variety of contexts. For example, application of US at high-peak rarefactional focal pressure (PRFP) has been shown to improve the delivery of antibodies to solid tumor xenografts when applied either before or during delivery of therapeutic antibody [9–11]. Specifically, Wang *et al.* used a fluorescently labeled antibody and microscopy analysis to show a 1.6-fold increase in net fluorescence signal within the sections from a US-treated tumor. Although this increase relied on application of a PRFP of 8.95 MPa and was shown to be nonsignificant and largely confined to the tumor periphery, the study did suggest the potential of the approach [10].

Indeed, it has since been shown that increased delivery of macromolecules to organ or tumor targets can be achieved, at much lower “diagnostic-like” PRFPs, when gas-entrapping nuclei are used to seed acoustic cavitation. Acoustic cavitation refers to a phenomenon whereby small vapor or gas bubbles within a fluid expand and contract as a result of the negative and positive pressure cycles of an US wave [12]. Cavitating bubbles can cause the surrounding fluid to flow, an effect termed “microstreaming,” which is thought to be a primary mechanism for US-mediated extravasation of drugs into solid tumors [13]. Cavitation can be largely classified as either inertial or noninertial, and although both types of cavitation can give rise to microstreaming, inertial cavitation has been shown to be more effective at transporting macromolecules [14]. In addition to microstreaming, the violent collapse of inertially cavitating bubbles can also give rise to shockwaves and microjets (reviewed in [13]), which can interact with vessel walls and impact on extravasation and delivery [15,16]. Inertial and noninertial cavitation events can be distinguished by the frequency spectra of their respective acoustic emissions (noninertial cavitation primarily

gives rise to emissions that are harmonics of the frequency of the delivered the US, whereas inertial cavitation emissions comprise a wide-range broadband frequency signal [12]. Crucially, these characteristic acoustic emissions can be used to temporally and spatially monitor and map cavitation using passive acoustic mapping (PAM), a US-based technique that can localize cavitating bubbles during therapy [17–21].

Delivery of therapeutic agents to the brain has proven a particularly attractive target for the US plus cavitation nuclei approach. In such studies, US has been used in conjunction with intravenously (iv.) administered microbubbles (typically US contrast agents [UCAs]) to temporarily open the blood–brain barrier (BBB) of a nontumor bearing animal and allow for extravasation of large macromolecules such as antibodies [22–25]. Kinoshita *et al.* showed that trastuzumab could be quantified in the brain in sites exposed to sonication with PRFPs of 0.6–0.8 MPa, whereas the level of trastuzumab in tissues not exposed to US was undetectable [22].

US at PRFPs on the order of approximately 1.5 MPa, in conjunction with iv. administered microbubbles, has been shown to enhance delivery of oncolytic viruses and liposomes [26–30]. Additionally, Dimceviski *et al.* showed that application of US at 0.27 MPa PRFP in conjunction with iv. delivered SonoVue microbubbles (Bracco, Italy) could be administered to patients receiving gemcitabine for pancreatic cancer treatment [31]. However, a key limitation identified in both the preclinical and human studies reported to date is the short circulation time and rapid destruction of microbubble UCAs necessitating repeated dosing to ensure sustained cavitation [26]. Moreover, as microbubbles have a diameter of several micrometers, they are generally too large to extravasate from blood vessels into the surrounding tumor tissue and therefore become spatially separated from the therapeutic they are required to impact. To address these limitations, gas-entrapping particles with a mean diameter of ~450 nm were developed by Kwan *et al.* to function in a similar role to UCAs and seed acoustic cavitation at relatively low PRFPs [32,33]. These sonosensitive particles (SonoTran Particles [SPs], OxSonics Therapeutics, Oxford, UK) were shown to sustain acoustic cavitation for greater durations than UCA microbubbles and enhanced delivery and efficacy of an oncolytic vaccinia virus [29,32]. Kwan *et al.* also provided initial qualitative histological evidence for improved delivery of a nontherapeutic dummy antibody using US and SPs. However, the scale of this effect has yet to be quantified, directly compared with delivery achieved with more conventional UCAs, or demonstrated with a therapeutic antibody capable of experiencing the binding site barrier [32]. Crucially, however, cavitation nucleated by SPs has been shown to not impact the structure or function of a range of anticancer drugs, including the therapeutic antibody cetuximab [34], the first step in demonstrating utility in enhancing the delivery of these agents.

Here we present the first quantitative analysis of delivery of a therapeutic antibody (cetuximab) to solid tumors outside of the brain with US-mediated cavitation. Delivery of cetuximab is examined in a bilateral xenograft tumor model in mice, and delivery achieved with cavitation seeded with either conventional SonoVue (SV, Bracco) microbubbles or with gas-stabilizing cup-shaped solid SPs is compared with delivery achieved after passive accumulation alone. This study provides evidence in support of further research of this noninvasive technique to increase site-specific delivery of this macromolecular drug.

Materials & methods

Tumor model

HT-29 cells (ATCC, UK) were cultured in high-glucose DMEM (11965-092, ThermoFisher Scientific, UK) supplemented with 10% fetal bovine serum (FBS; 10270-106, ThermoFisher Scientific, UK) and were incubated at a temperature of 37°C in 5% CO₂. Female CD-1 nude mice (CrI:CD1-Foxn1nu [086], Charles River, UK) were housed and cared for according to UK Home Office guidelines and the UKCCCR Guidelines for the Welfare of Animals in Experimental Neoplasia. Sixteen mice were implanted with tumors. Mice were housed in individually vented cages of no more than 10 mice, and welfare checks and weighing were performed every 3–4 days. Cages were provided with ALPHA-Dri bedding (1032003, LBS Biotech, UK) with shredded paper and plastic or card tunnels for enrichment. Water and food (RM3 801700, Special Diet Services, Essex, UK) was provided ad libitum. Humidity was kept at 45–60%, the temperature was maintained at 20–24°C and light levels were kept low with a light/dark cycle of 12/12, while extraneous noise was minimized. Mice were inoculated subcutaneously on each flank with an injection of 3×10^6 HT-29 cells, resuspended in serum-free DMEM. US treatment was performed when mice had two well-matched tumors with volumes of approximately 100 mm³ (measured by calipers and calculated as half the product of length, width, and depth).

US apparatus & parameters

Two confocally aligned focused US (FUS) transducers (single element, spherically focused, fundamental frequency = 0.5 MHz, focal length = 63 mm, outer diameter = 64 mm: H-107C, Sonic Concepts, Bothell, WA, USA) were mounted orthogonally to each other in a water tank heated to 37°C. The water was degassed through a circuit consisting of a centrifugal pump, deionization column, 10-μm filter and vacuum degassing membrane. Successful degassing was confirmed by insonating the water tank with the FUS transducers and ensuring no cavitation acoustic emissions were detected. Each FUS transducer contained a rectangular cutout (45 × 18 mm), housing L11-5v 128-element linear arrays (center frequency = 6.25 MHz, aperture = 38 mm, bandwidth = 5–11 MHz: Verasonics Inc., Kirkland, WA, USA). The linear arrays were mounted within the FUS transducers such that the FUS foci were within the elevational plane of the arrays. Custom software written in MATLAB on a Vantage Verasonics 256 research platform (Verasonics Inc.) was used to initiate the US pulses and record data from the linear arrays. Specifically, the Verasonics sent an output trigger pulse to a signal generator (33250A, Agilent, Wokingham, Berkshire, UK), which output to a 55 dB power amplifier (1040L, Electronics and Innovation, Rochester, NY, USA), which in turn output to the FUS transducers through impedance matching networks (Sonic Concepts) (Supplementary Figure 1). The Verasonics research platform was also used to create a custom algorithm that interleaved active B-mode US imaging with the passive acoustic data recording. During treatment, the active B-mode US imaging was used to visualize the tumor and ensure correct FUS targeting. The passive acoustic data recorded was beamformed using a proprietary algorithm to provide an estimate of the cavitation energy in the target region.

Dosing & US exposures

Anesthesia was induced using 5% isoflurane in O₂, and maintained with 2.0–2.5% isoflurane in O₂ (achieved using an AW Anesthesia Services Limited rig [Stoke, UK] with a Nidek Nuvolite Oxygen concentrator [Birmingham, AL, USA]). Once mice were anesthetized,

a cannula was placed and secured into the tail vein. Mice were then mounted onto a custom-made platform, and placed in a 37°C water tank, where the orthogonal FUS transducers were aligned onto one of the flank tumors using B-mode imaging (Supplementary Figure 1). Alignment of the target tumor so that it protruded beyond the body of the mouse, and placement of the US focal region entirely within the tumor ensured other areas of the mouse were not exposed to FUS. At the onset of US treatment, each mouse received a dose of 5 µg of cetuximab in one bolus injection of 25 µl of PBS. One group of mice (n = 4) also received 50 µl of SV resuspended in PBS according to manufacturer's instructions; the second group of mice received a 1.1-mg dose of SPs, manufactured as described by [32], in 50 µl of 5% glucose in sterile water. The dose of SV was split into two injections: 25 µl at onset of treatment, and 25 µl after 4 min of treatment, to mitigate the rapid clearance of SV. The full dose of SPs was given in one bolus injection immediately following the injection of cetuximab. The amount of gas administered in the doses of SV and SPs was ~20 and 60 nanomoles, respectively (calculated as described by Mannaris *et al.* [35]). The focal volume of the orthogonally mounted FUS transducers is described at –6 dB by the product of 6.2 × 1.4 × 3.4 mm (axial x lateral x elevation) and at –3dB by 4.4 × 1.0 × 2.4 mm. Because this focal volume was small compared with the average tumor volume (~120 mm³), before treatment, B-mode imaging was used to identify the tumor limits in three dimensions. A three-axis manual positioning system (Newport, Irvine, CA, USA) was then used to manually move the mouse platform during treatment so the entire tumor was treated with FUS. Real-time cavitation monitoring (as shown in Supplementary Figure 4) allowed feedback on the tumor regions that had cavitation activity and those which did not and therefore required further exposure. The input voltage to the FUS transducers was adjusted during treatment to give PRFPs between approximately 1.5 and 2.0 MPa in response to the acoustic feedback from the linear array transducers. FUS transducers were driven at their fundamental frequency of 0.5 MHz, with a pulse repetition frequency of 0.5 Hz and a duty cycle of 5% (50,000 cycles per burst). US treatment was performed for 600 s, after which time the mice were removed from the water tank and sacrificed. Tumors were recovered for quantification of cetuximab; tumors were rinsed twice in PBS after dissection, frozen and stored at –80°C until analysis. Approximately 12 min passed between injection of cetuximab and sacrifice of mice. Please see the Supplementary Methods section for a description of the methods employed to generate the data for Supplementary Figure 5.

Analysis of acoustic data

Details of the algorithm used for passive acoustic mapping are described by Coviello *et al.* [21], and its specific implementation in the context of an orthogonal dual array setup is described by Gray *et al.* [36]. The cavitation data from the first 200 µs of each 100 ms US pulse was recorded and analyzed. Then, for every PAM frame (acquired approximately every 2 s), the maximum cavitation energy (in arbitrary units, denoted as PAM magnitude) was extracted and plotted over time. This metric was used to adjust input FUS voltage during treatment to minimize variability between mice and keep PAM magnitude between approximately 10 and 20 (arbitrary units).

ELISA quantification

Frozen tumors were weighed, diced with a scalpel, and suspended in 1x cell culture lysis

reagent (E1531, Promega, Hampshire, UK) with protease inhibitor cocktail (ab65621, Abcam, Cambridge, UK) to a concentration of 40 mg/ml (1:500 dilution of protease inhibitor cocktail), then thoroughly homogenized. Control tumor homogenate was prepared from tumor-bearing mice that did not receive any cetuximab, and this homogenate was spiked with serial dilutions of known amounts of the cetuximab injectate to create standards from which to quantify the samples.

Ninety-six-well Nunc Maxisorp plates (44-2404-21, ThermoFisher Scientific, UK) were coated overnight (4°C) with 1 µg/ml anti-human antibody (A9544, Sigma-Aldrich, UK) in bicarbonate buffer (C3041-50, Sigma-Aldrich, UK). After coating, plates were washed 5x with a solution of PBS + 0.05% Tween-20 (wash buffer), then blocked for 1 h with 10% FBS in PBS. After blocking (and one rinse with wash buffer), plates were incubated with 50 µl of sample/standard (in triplicate) for 2–4 h, then washed 5x with wash buffer. Plates were then incubated with an anti-human horseradish peroxidase-conjugated antibody (W4031, Promega, Hampshire, UK) at a dilution of 1:2500 in 10% FBS in PBS for 1 h. After 5x washing, plates were incubated with TMB substrate (34029, ThermoFisher Scientific, UK), and incubated in the dark until a definitive color change from clear to blue was observed for the highest concentration standards. At this point, development was stopped with addition of 0.5 M sulphuric acid, and absorbance of the wells was measured at 450 nm using a plate reader (FLUOstar Omega, BMG Labtech, Aylesbury, Bucks, UK). Absorbance values of standard curve were fit in GraphPad Prism (version 7), and sample values were extrapolated from this fit.

Statistical analysis

All acoustic feedback data metrics were analyzed by way of two-sided unpaired t-tests in Graphpad Prism (version 7).

A linear mixed model was used to analyze antibody delivery data, with cavitation nuclei, US and their interaction as fixed effects and a random intercept to model the correlation between tumors within the same mouse. Because ELISA data are typically affected by proportional error, the data were log-transformed to stabilize the variance [37]. The log-transformed concentrations were fitted using the *lmer* function of the *lme4* package [38] in R [39]. 95% CIs and p-values for *post hoc* tests were estimated using the Satterthwaite approximation for the degrees of freedom. Means and CIs were estimated on the log scale and then back-transformed to the response scale; as a consequence, all means are reported as geometric means. Statistical tests on ratios were performed on the log scale, and all p-values were corrected for multiple comparison using the Holm-Bonferroni method. The significance of the interaction term in the linear models was assessed with an F test, using the Satterthwaite approximation for the denominator degrees of freedom [40].

Because no departure from linearity was observed in the dependence of concentration on cumulative PAM magnitude, heteroskedasticity was taken into account in that model by weighting rather than log-transformation. The data were modeled by generalized least squares, with cavitation nuclei, PAM magnitude and their interaction as predictor variables, using the *gls* function in the *nlme* package in R [41], with a compound symmetry correlation structure to model the correlation between tumors in the same mouse, and weights obtained from the inverse of the square root of fitted squared residuals. All p-values were two-sided, and the significance level for all tests was set at 0.05.

Results

Acoustic feedback & passive acoustic mapping

During US treatment, cavitation activity was monitored by PAM [18–20,42]. The cavitation data from the first 200 μ s of each 100 ms US pulse was recorded and analyzed. Cavitation events were detected passively by the orthogonal linear arrays [43], and source locations were mapped (representative image shown in Supplementary Figure 4). As a measure of cavitation energy, PAM magnitude (the maximum energy pixel extracted from each PAM map) was followed in real time, with cavitation levels between 10 and 20 arbitrary units being deemed the target cavitation dose to increase reproducibility between mice by delivering an equivalent “dose” of cavitation. FUS transducer pressure was adjusted in real time accordingly and varied between approximately 1.5 and 2.0 MPa PRFP. Figure 1 shows representative traces of PAM magnitude over time during US treatment with SV (panel A) or with SPs (panel B). Panel A shows the short-lived nature of cavitation nucleated by SV because the micron-sized bubbles are cleared rapidly from circulation [44] and therefore had to be replenished with a second dose partway through US exposure. Conversely, the SPs (panel B) showed relatively sustained cavitation, with events detected throughout the 600 s treatment following a single bolus injection. These cavitation profiles are in agreement with previous preclinical [26,28,29,32] and clinical [31] experience.

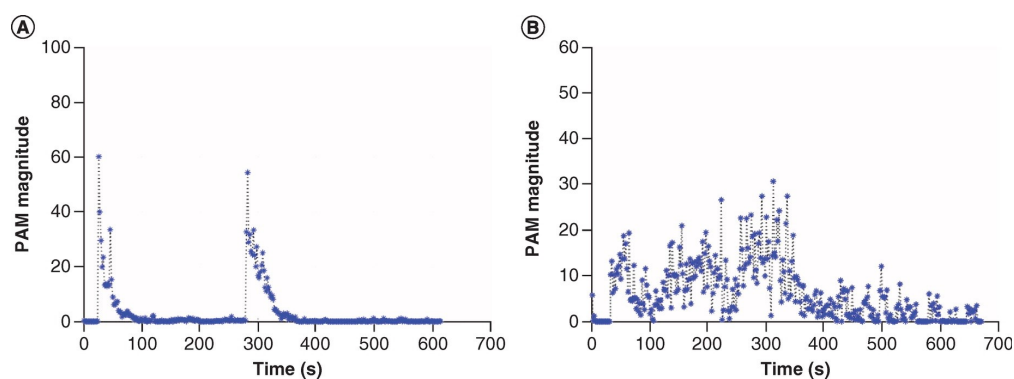


Figure 1. Representative acoustic feedback data acquired during ultrasound treatment of tumors from mice dosed with (A) SonoVue or (B) SonoTran particles.

Mice dosed with SonoVue (A) received the dose in two bolus injections of 25 μ l, one at the onset of treatment, and the second 240 s later. Mice dosed with SonoTran particles (B) received one bolus injection of 1.1 mg SonoTran particles at the onset of treatment. Each data point represents the maximum value pixel extracted from the corresponding frame of PAM throughout the 600 s ultrasound exposure. PAM magnitude units are calculated with a proprietary algorithm and reported in arbitrary units that are proportional to the acoustic energy recorded during each focused ultrasound pulse. Profiles for all mice are shown in the supplementary data (Supplementary Figure 2).

PAM: Passive acoustic mapping.

The observations from Figure 1 are quantified in Figure 2, where maximum and cumulative (integrated) PAM magnitudes (Figure 2A and B), as well as the percentage of US exposure time spent above a threshold of PAM magnitude (Figure 2C) are compared for SV and SPs. Note that US exposure time refers to 5% of the total treatment time (600 s), as an US duty cycle of 5% was used here.



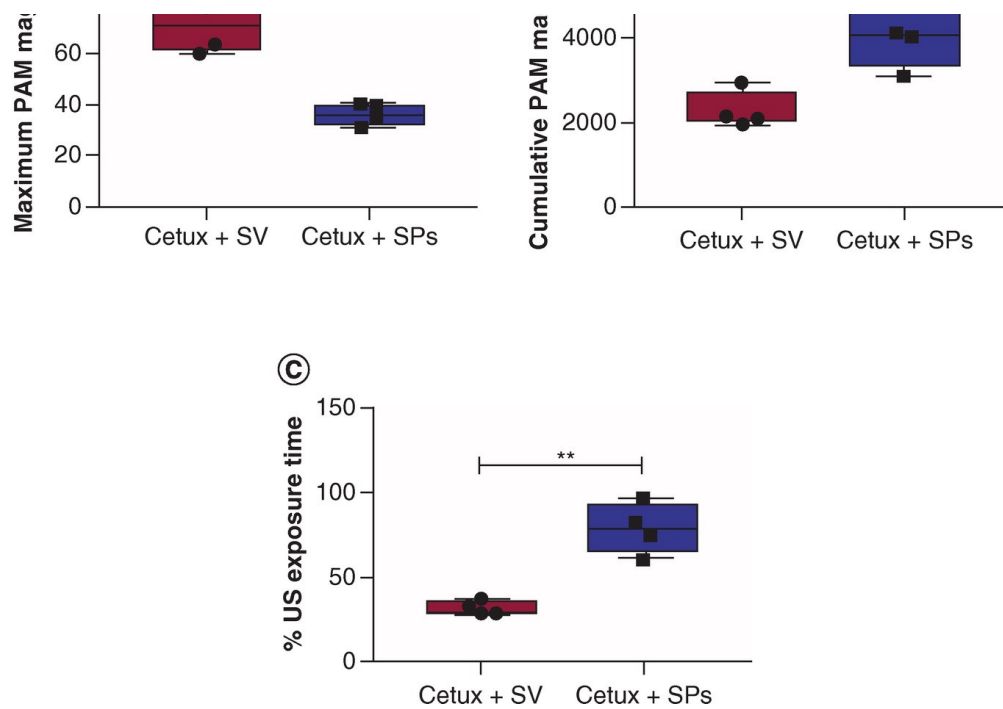


Figure 2. Quantification of acoustic feedback data acquired during ultrasound treatment of tumor-bearing mice treated with cetuximab and cavitation nuclei (SonoVue or SonoTran particles).

(A) Maximum PAM magnitude recorded during treatment, (B) cumulative PAM magnitude integrated over treatment time (600 s), (C) percentage of US exposure time during which PAM magnitude was above a threshold value of 1 (essentially any signal above the background level). Box-and-whisker plots show median, first and third quartiles, and maximum and minimum values (points denote values from individual mice, $n = 4$). Statistical significance was assessed with unpaired two-sided t-tests. ** $p < 0.01$.

Cetux: Cetuximab; PAM: Passive acoustic mapping; SP: SonoTran particles; SV: SonoVue.

Although the maximum PAM magnitude achieved was significantly greater for mice treated with SV than with SPs (Figure 2A), cavitation persistence was significantly greater with SPs (Figure 2C). The cumulative, or total cavitation energy (as measured by PAM magnitude) was significantly greater in tumors receiving SPs than SV (Figure 2B).

As cavitation was more sustained for the SPs + US treatment group, it is possible that this also caused an increased occurrence of cavitation and a consequent low level of bruising in the skin or at the surface of surrounding tissue (Figure 3). When tumors were excised post-US treatment, they were rinsed twice in PBS to mitigate the potential confounding effects of blood from surrounding skin remaining associated with tumors.

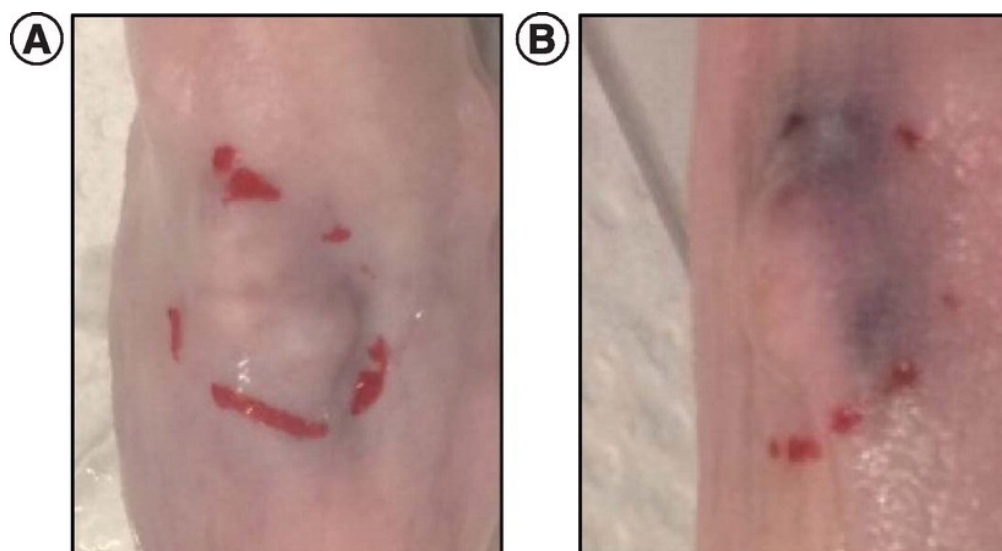


Figure 3. Representative photographs of tumors immediately after ultrasound treatment in mice receiving (A) SonoVue or (B) SonoTran particles as cavitation nuclei.

Red demarcates the tumor boundaries. All ultrasound-treated tumors for mice receiving SonoTran particles ($n = 4$) are shown in Supplementary Figure 3.

Quantification of tumoral antibody delivery

The percentage of the injected dose (ID) of cetuximab that was recovered associated with the excised tumors was quantified using a sandwich ELISA, with anti-human antibodies as both capture and secondary antibodies. The concentration of cetuximab (% ID/g tissue) in samples of each homogenized tumor was quantified using a standard curve made with untreated tumor homogenate spiked with the injectate of cetuximab. The concentrations were log-transformed to stabilize the variance (because ELISA measurements are typically affected by proportional error [37]) and fitted to a linear mixed model with US, type of cavitation nuclei and their interaction as fixed effects and mouse (subject) as a random intercept to model the correlation between tumors within the same mouse.

The type of cavitation nuclei did not influence delivery of cetuximab in the absence of US exposure (1.1-fold increase for SPs vs SV without US, 95% CI 0.7–1.8, $p = 0.6$). Approximately 1.5% of the injected dose/g of tumor (~70–80 ng of cetuximab/g tumor) was recovered regardless of whether SV or SPs were injected. This suggests that (within the timeframe evaluated here) the impact of these cavitation nuclei on passive accumulation of cetuximab is negligible.

Application of US-mediated cavitation was found to increase tumoral concentration of cetuximab (% of ID/g of tumor) in 8 of 8 mice (Figure 4). Cavitation nucleated by SPs was found to lead to 1.9 times greater mean concentration (% ID/g tumor) of cetuximab than cavitation nucleated by SV (95% CI 1.2–3.1, $p = 0.02$). For mice receiving SV, there was 2.1-fold (95% CI 1.3–3.4, $p = 0.02$) more cetuximab found in the US-treated tumor, whereas a 3.6-fold (95% CI 2.3–5.8, $p = 0.002$) increase with US-treatment was found for mice receiving SPs.

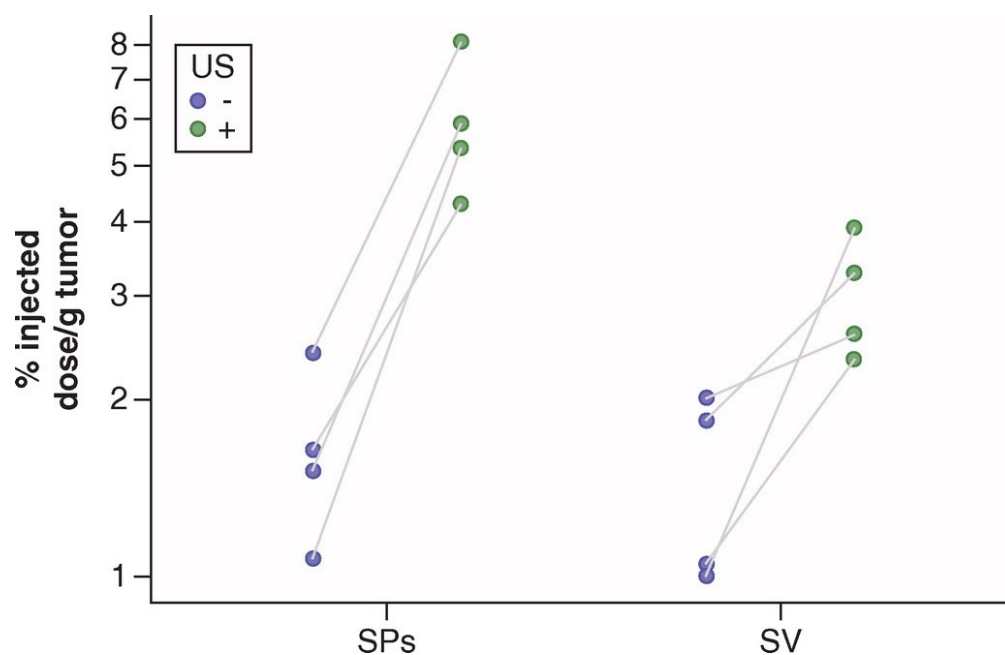


Figure 4. Quantification of tumoral concentrations of cetuximab, with and without exposure to ultrasound-mediated cavitation.

Blue points denote tumors that were not exposed to US (cetuximab + SV or SPs only), whereas green points

denote tumors which received 10 min of US exposure (cetuximab + SV or SPs + US). Bilateral tumors from the same mouse are linked by a gray line.
SP: SonoTran particles; SV: SonoVue; US: Ultrasound.

Although the antibody concentration in the US-treated tumors was significantly greater for SPs than SV, the interaction between cavitation nuclei and US (i.e., the ratio between the US-induced concentration fold change for different cavitation nuclei) was estimated as 1.7 (95% CI 0.9–3.3, $p = 0.09$) and was not statistically significant. The wide confidence interval around this estimate, which encompasses values that may be therapeutically relevant, suggests that a larger sample size would be needed to assess the effect of cavitation nuclei on the US dependence of antibody delivery to tumors. See [Tables 1](#) and [2](#) for a summary of model estimates.

Table 1. Estimated marginal means of linear mixed model and 95% CIs of delivered dose for all experimental groups. (Table view)

Cavitation nuclei	Ultrasound	Mean (95% CI)	
		µg/g	%ID/g
SonoVue	–	0.07 (0.05–0.10)	1.4 (1.0–2.0)
	+	0.15 (0.11–0.21)	3.0 (2.1–4.1)
SonoTran Particles	–	0.08 (0.06–0.11)	1.6 (1.1–2.2)
	+	0.30 (0.21–0.40)	5.8 (4.1–8.0)

Table 2. Effect of ultrasound and cavitation nuclei on tumoral concentration of cetuximab. (Table view)

Comparison		Fold-change (95% CI)	p-value
Effect of ultrasound (+ vs –)	SV	2.1 (1.3–3.4)	0.03
	SPs	3.6 (2.3–5.8)	0.002
Effect of cavitation nuclei (SPs vs SV)	+ US	1.9 (1.2–3.1)	0.03
	– US	1.1 (0.7–1.8)	0.6

SP: SonoTran particles; SV: SonoVue; US: Ultrasound.

Relationship between acoustic feedback & quantification of delivery

In the analysis presented thus far, US was modeled as a categorical variable with two levels (+ and –). As shown in [Figures 1](#) and [2](#), however, a variety of metrics can be extracted from the acoustic feedback (PAM maps) acquired during US treatment. While viewing US treatment as a binary variable allowed for relevant comparisons between treatment groups to be made, the acoustic data acquired (and variability in this data between mice) suggest that US treatment can be modeled as a continuous predictor. Using a continuous metric of cavitation activity in the model rather than a categorical predictor could give more physical meaning to the parameters estimated by the model [\[45\]](#) and help further elucidate the relationship between cavitation activity and drug delivery.

The cumulative PAM magnitude ([Figure 2B](#)) was calculated by integrating the magnitude of the maximum value pixel from each recorded PAM frame over the duration of US treatment; this metric is thus determined by both PAM magnitude and duration and is in

fact representative of the total energy of broadband acoustic emissions associated with cavitation over the course of a whole treatment. **Figure 5** shows the fit of the new model with cumulative PAM magnitude as a continuous predictor of cetuximab concentration (note that tumors that did not receive US treatment were assigned a cumulative PAM magnitude of 0).

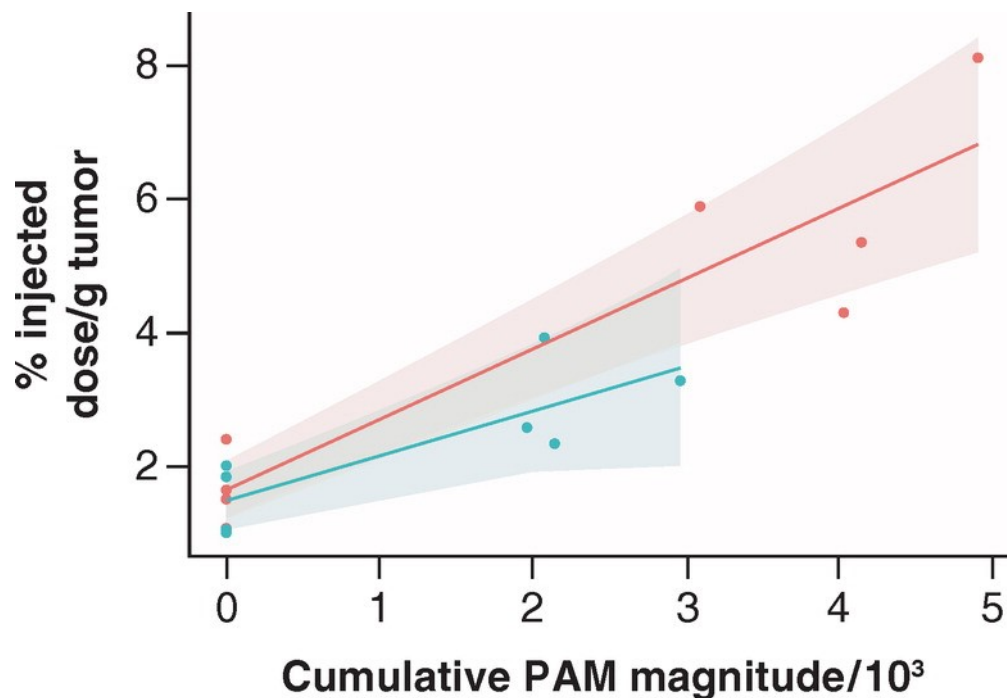


Figure 5. Tumoral cetuximab concentration as a function of cumulative passive acoustic mapping magnitude for SonoTran particles (red) and SonoVue (green).

Continuous lines show the fit (shading represents 95% CI), whereas points show data from individual mice ($n = 4$ per cavitation nuclei type, two tumors per mouse). Note that “cumulative PAM magnitude” is an arbitrary unit derived from extracting the maximum energy pixel from each PAM map and integrating over time. $\chi^2_v = 2.7$.

PAM: Passive acoustic mapping.

To investigate the effect of cumulative PAM magnitude on antibody delivery, the concentration of antibody in the tumor was regressed on cumulative PAM magnitude using a generalized least squares model to take into account the correlation between measurements in the same mouse and the proportional error of the ELISA readings.

The effect of cumulative PAM magnitude on antibody delivery (the slopes of the regression lines in **Figure 5**) was estimated as $0.7 \cdot 10^{-3}$ % ID/g per unit of PAM magnitude (95% CI $0.1 \cdot 10^{-3}$ – $1.3 \cdot 10^{-3}$, $p = 0.025$) for SV and $1.1 \cdot 10^{-3}$ % ID/g per unit of PAM magnitude (95% CI $0.7 \cdot 10^{-3}$ – $1.4 \cdot 10^{-3}$, $p = 0.0001$) for SPs. The impact of cavitation nuclei on the effect of PAM magnitude (i.e., the difference between slopes corresponding to different nuclei) was estimated as $0.4 \cdot 10^{-3}$ % ID/g per unit of PAM magnitude (95% CI $-0.3 \cdot 10^{-3}$ – $1.1 \cdot 10^{-3}$, $p = 0.3$) and was not statistically significant. As in the model with US as a categorical variable, the wide CIs around this estimate, which encompass differences that may be therapeutically relevant, suggest that a larger sample size would be needed to investigate a potential effect of cavitation nuclei on the cumulative PAM magnitude dependence of antibody concentration in tumors.

Notably, because cavitation activity was only recorded and analyzed from the first 200 μ s of each 100 ms US pulse, it is possible that the metric of PAM magnitude presented

here underestimates the true amount of cavitation nucleated by the SPs relative to SV, as the SV microbubbles are expected to be rapidly destroyed by the US pulse [46], whereas SPs generally produced more sustained cavitation emissions.

These results suggest, nevertheless, that cumulative PAM magnitude (as a measure of cavitation activity) may correlate with antibody delivery, regardless of the type of nuclei used to seed cavitation. More refined capture and spatial mapping of the PAM data will be required to strengthen the robustness of this relationship.

Discussion

In all mice treated with US-mediated cavitation, a greater percentage of the ID of cetuximab was recovered from the US-treated tumor than from the tumor exposed only to circulating antibody and cavitation nuclei but no US. The ELISA method employed here for quantification of cetuximab allowed for precise determination of total tumoral concentration and ultimately the %ID/g of tumor, unlike some commonly used imaging-based quantification methods such as immunohistochemistry, which are necessarily limited to quantification in select regions of the tumor.

The concentration of antibody delivered to the US-treated tumors was 1.9 times greater for mice in which cavitation was nucleated by the SPs, which entrap a nanobubble of gas in a hemispherical cup shape [32,33] than by the commercial SV micron-scale bubbles. The mean amount of antibody delivered to tumors using US and SPs as cavitation nuclei was $0.30 \pm 0.08 \mu\text{g/g}$ of tumor (ID of $5 \mu\text{g}$). This compares favorably with results of Luo *et al.*, who estimated a delivery of just over $0.5 \mu\text{g}$ of cetuximab/g of tumor to mouse xenografts (GEO cells) after 24 h of passive accumulation (reflecting the maximum tumoral concentration measured after intraperitoneal administration of a dose of $40 \mu\text{g}$ of cetuximab) [47]. Notably, the fold-increase in delivery mediated by SV-nucleated cavitation is in excellent agreement with that calculated by Carlisle *et al.* for delivery of an polymer-coated adenovirus with SV + US, when quantitative PCR was used to quantify virus particles 24 h after delivery [27]. Work by Miyamoto *et al.* demonstrated that heating of stroma-rich tumors could enhance delivery of cetuximab up to 4.8-fold [48], whereas combination of tumor-targeting antibody therapy (trastuzumab) with vascular normalization was shown to actually impede delivery [49,50].

The difference in delivery between SV and SPs is likely due to the greater persistence of cavitation nucleated by SPs, giving rise to a potentially greater “dose” of cavitation energy (approximated here by cumulative PAM magnitude). The US settings were chosen to generate inertial cavitation with both SPs and SV. The parameters match those used in previous studies where improved delivery with SV [26–28] and SPs [29] was shown. Bazan-Peregrino *et al.* showed *in vivo* that inertial cavitation can be generated from SV with a US frequency of 0.5 MHz, 1.2 MPa PRFP, 0.5Hz PRF and 6% duty cycle, whereas insonation with a PRFP of only 0.36 MPa gave rise to harmonic emissions, suggesting noninertial cavitation, and minimal drug delivery. It was shown previously *in vitro* that inertial cavitation with SV is sensitive to PRF because bubbles are destroyed with insonation, and thus matching the interval between pulses (PRF) to reperfusion time was key. Bazan-Peregrino *et al.* showed *in vivo* that reperfusion time of ZR75.1 xenograft tumors was approximately 4 s, and so a PRF of 0.5 Hz (pulse interval of 2 s) was chosen to match the half-perfusion time to allow for bubble replenishment between pulses.

The sustained cavitation seen with SPs may relate to enhanced circulation kinetics and

sustained bloodstream concentrations (compared with the rapidly cleared SV), although previous pharmacokinetic profiling in mice suggests that by 10 min SP blood levels may have dropped by 80%, a sufficient drop to expect a consequent reduction in cavitation level [32]. This raises the question of how cavitation in the tumor may outlast high bloodstream concentrations of SPs. This phenomenon may be explained by SPs achieving cavitation-mediated passage into the tumor mass and therein continuing to nucleate further cavitation. This possibility is supported by the presence of SPs detected in tumors after US exposure (Supplementary Figure 5) and the evidenced ability of SPs to nucleate sustained cavitation [51].

Future studies with this technology should investigate the effects of the enhanced delivery to the tumor region shown here on therapeutic efficacy of cetuximab (or other antibody therapeutics). Additionally, to optimize the enhanced delivery observed here, it would be of use to probe the impact of altered pulse lengths, pressures, and durations of US exposure in future experiments. Studies should also include detailed characterization of the mechanical effects of US-mediated cavitation on surrounding tissue, tumor vasculature and tumor growth/size in the absence of therapeutic drug.

Compared with passive delivery over 12 minutes of circulation, treatment with US-mediated cavitation was able to increase the amount of therapeutic delivered in all mice treated. Although treatment with US-mediated cavitation has cost implications and technical challenges compared with simple iv. infusion, these results highlight several potential benefits that warrant further consideration. First, initial cavitation-mediated antibody delivery achieved after 12 min does not preclude further passive accumulation of antibody thereafter and so may provide an even greater level of antibody delivery after longer circulation times. Second, it has been shown with replicating oncolytic viruses that small increases in net delivery with US-mediated cavitation can lead to large increases in virus replication and therapeutic transgene production, an effect which has been attributed to better penetration and distribution of virus [27]. As multiple preclinical studies have shown, antibody delivery to solid tumors is heterogeneous, particularly at early time points following delivery and with low doses of antibody [4–6]. Clinically, Lu *et al.* showed that there is significant variation in tumor delivery of an anti-EGFR antibody between patients and between lesions within the same patient. Moreover, tumor size was shown to have predictive value for intratumoral antibody accumulation, with larger tumors having lower concentrations of antibody and with antibody preferentially distributed peripherally within lesions, often regardless of the level of EGFR expression [8]. Thus, it may be that an advantage of the “burst” antibody delivery achieved with US-mediated cavitation compared with slow passive accumulation, could be improved spatial distribution. In support of this, Kwan *et al.* provided evidence of improved antibody distribution as a result of SP-mediated cavitation [32], although as the antibody used was a dummy IgG, the work did not provide proof that the binding site barrier can be overcome using cavitation. To extend the work reported here, immunohistochemical analysis of distribution of the cetuximab would be an important next step. A third important finding of this work is that although passive accumulation of antibody is highly variable and may not even be predictable from tumor perfusion rates (which themselves fluctuate markedly and are hard to predict), cavitation may provide a more consistent approach to delivery. It is known that great heterogeneity in clinical responses to drugs such as cetuximab are evident, not all of

which can be ascribed to EGFR expression [52] or *KRAS* status [53–55]. The differences in intratumoral pressure [56], extracellular matrix density and tumor perfusion between different regions of the same tumor [57], different tumors in the same patient and tumors in different patients, make achieving a standard predictable intratumoral dose challenging. The data presented here indicate that US-mediated cavitation may help address this.

Although the challenge of achieving effective and homogenous delivery of therapeutics into and throughout solid tumors is now well recognized [58,59], options to meet this challenge are limited. Vascular normalization can be used to restore vessel functionality and convective flow across tumors and has been shown to benefit the delivery of small molecules [60,61]. However, vascular normalization may lead to a removal of the “leaky” vasculature in tumors and thereby ultimately impede the delivery of larger nanomedicines such as viruses, liposomes and antibodies [49,50,62,63]. Recent murine studies using an oncolytic virus provided an elegant demonstration of how alterations to systemic blood pressure (with exercise or anesthesia) can have an impact on tumor uptake [64], although standardizing and clinically translating such observations could be a challenge. Endeavors to assist tumoral drug uptake using external stimuli to generate heat or cavitation events have also gained much research focus [10,23,27,65–67]. Although the targeted heating of tumors at depth can be hard to control and may require the deposition of large amounts of energy and therefore expensive and scarce equipment [68], instigation of US-mediated cavitation events is potentially more broadly and cheaply applicable. The SPs and US technology described here provides a promising means of turning this potential into a clinical reality. Future studies can address whether the enhanced delivery of antibody provided by cavitation can ultimately lead to enhanced therapeutic efficacy.

Conclusion

To date, cetuximab has shown limited efficacy as a single agent in the treatment of metastatic colorectal cancer (response rates of approximately 11%) [52,54,55] and is most effective when administered in combination with other chemotherapeutics [52,53]. Novel methods for improving the efficacy of cetuximab and other macromolecular biologic therapeutics are clearly needed. US-mediated cavitation, nucleated by either SPs or SV, gave an immediate increase in the total amount of cetuximab delivered to solid tumor xenografts. This provides the first demonstration of a quantifiable increase in the level of therapeutic antibody delivered to a xenograft tumor outside of the brain using US-mediated cavitation.

Summary points

- Intratumoral delivery of systemically delivered therapeutic antibodies has been shown to be heterogeneous, especially at low doses and early time points.
- Ultrasound-mediated cavitation can be used to site-specifically enhance the delivery of macromolecular drugs such as oncolytic viruses or liposomes.
- Cavitation can be nucleated at low peak-rarefactional focal pressures using micrometre-sized ultrasound contrast agents, or alternatively by nanoscale gas-entrapping particles.
- It was shown that ultrasound-mediated cavitation increases the concentration of cetuximab recovered from an ultrasound-treated tumor, compared with an untreated control tumor receiving only intravenous cetuximab and cavitation nuclei (tumoral delivery of the therapeutic antibody cetuximab was directly quantified using an ELISA).

- Greater levels of tumoral cetuximab concentration were achieved using gas-entrapping nanoparticles as cavitation nuclei than with micrometre-sized US contrast agent.
- Analysis of passively acquired acoustic cavitation signals shows a correlation between total recorded cavitation energy and tumoral cetuximab concentration.

Supplementary data

To view the supplementary data that accompany this paper please visit the journal website at: www.futuremedicine.com/doi/suppl/10.2217/hnm-2020-0263

Author contributions

M Grundy contributed significantly to the design of the experiments and analysis presented here, performed all experiments described in this manuscript, analyzed all data acquired and was the primary drafter of the manuscript. L Bau contributed significantly to the analysis of the data presented here and helped revise the manuscript. C Hill worked with M Grundy to process all tissue from the *in vivo* ultrasound experiments presented here, helped to analyze the acquired acoustic data and helped to revise the manuscript. C Paverd operated the ultrasound setup during the *in vivo* ultrasound experiments, helped to analyze the acquired acoustic data and helped to revise the manuscript. C Mannaris assisted with acoustic data analysis and revised the manuscript. J Kwan performed experiments and analyzed data pertaining to Supplementary Figure 5. C Crake designed and implemented software and hardware for the capture and processing of cavitation data and helped revise the manuscript. C Coviello designed and implemented software and hardware for the capture and processing of cavitation data and helped revise this manuscript. C Coussios contributed significantly to the design of the experiments presented here, provided guidance on the analysis and interpretation of the acoustic data and helped revise the manuscript. R Carlisle contributed significantly to the design of experiments presented here, worked on the *in vivo* experiments presented here, contributed to the analysis of data and contributed significantly to the drafting and revision of the manuscript.

Acknowledgments

Dr. Megan Jackson and Dr. Rachel Myers of OxSonics Therapeutics are acknowledged for their assistance with development of the ELISA protocol used here.

Financial & competing interests disclosure

This research was supported by the Clarendon Fund (M Grundy), and the Engineering and Physical Sciences Research Council (EPSRC) under Programme Grant EP/L024012/1 (OxCD3: Oxford Centre for Drug Delivery Devices) (R Carlisle, C Coussios, C Mannaris, L Bau, C Paverd, C Hill, M Grundy). R Carlisle, C Coviello and C Coussios are founders and shareholders in OxSonics Therapeutics, which holds intellectual property relating to the polymeric sonosensitive particles and ultrasound technology used in these experiments. C Crake is an employee of OxSonics Therapeutics. M Grundy and C Mannaris consulted to OxSonics Therapeutics on a separate project at the time of data collection and have no financial interest in OxSonics Therapeutics. J Kwan was previously employed at OxSonics Therapeutics and holds intellectual property relating to the polymeric sonosensitive particles. The authors have no other relevant affiliations or financial involvement with any organization or entity with a financial interest in or financial conflict with the subject matter or materials discussed in the manuscript apart from those disclosed.

No writing assistance was utilized in the production of this manuscript.

Ethical conduct of research

The authors state that they have obtained appropriate institutional review board approval or have followed the principles outlined in the Declaration of Helsinki for all human or animal experimental investigations. Animal experiments were performed in accordance with institutional and UK Home

Office (HO) guidelines under a HO approved animal license, in Home Office approved facilities by staff with HO personal licenses.

Open Access

This work is licensed under the Attribution-NonCommercial-NoDerivatives 4.0 Unported License. To view a copy of this license, visit <http://creativecommons.org/licenses/by-nc-nd/4.0/>

References

Papers of special note have been highlighted as: • of interest; •• of considerable interest

1. Glassman PM, Balthasar JP. Mechanistic considerations for the use of monoclonal antibodies for cancer therapy. *Cancer Biol. Med.* 11(1), 20–33 (2014). [PubMed](#).
2. Chauhan VP, Stylianopoulos T, Boucher Y, Jain RK. Delivery of molecular and nanoscale medicine to tumors: transport barriers and strategies. *Annu. Rev. Chem. Biomol. Eng.* 2, 281–298 (2011). [Crossref](#). [PubMed](#).
3. Juweid M, Neumann R, Paik C et al. Micropharmacology of monoclonal antibodies in solid tumors: direct experimental evidence for a binding site barrier. *Cancer Res.* 52(19), 5144–5153 (1992). [PubMed](#).
4. Baker JH, Lindquist KE, Huxham LA et al. Direct visualization of heterogeneous extravascular distribution of trastuzumab in human epidermal growth factor receptor type 2 overexpressing xenografts. *Clin. Cancer Res.* 14(7), 2171–2179 (2008). [Crossref](#). [PubMed](#).
5. Lee CM, Tannock IF. The distribution of the therapeutic monoclonal antibodies cetuximab and trastuzumab within solid tumors. *BMC Cancer.* 10(1), 255 (2010). [Crossref](#). [PubMed](#).
6. Baker JHE, Kyle AH, Reinsberg SA et al. Heterogeneous distribution of trastuzumab in HER2-positive xenografts and metastases: role of the tumor microenvironment. *Clin. Exp. Metastasis.* 35(7), 691–705 (2018).
 •• This study characterized the heterogeneous distribution of a therapeutic antibody in mouse xenografts and metastases and examined this distribution in relation to important tissue and vascular barriers to antibody delivery.
[Crossref](#). [PubMed](#).
7. Cruz E, Kayser V. Monoclonal antibody therapy of solid tumors: clinical limitations and novel strategies to enhance treatment efficacy. *Biol. Targets Ther.* 13, 33–51 (2019). [Crossref](#).
8. Lu G, Fakurnejad S, Martin BA et al. Predicting therapeutic antibody delivery into human head and neck cancers. *Clin. Cancer Res.* 26(11), 2582–2594 (2020). [Crossref](#). [PubMed](#).
9. Khaibullina A, Jang B-S, Sun H et al. Pulsed high-intensity focused ultrasound enhances uptake of radiolabeled monoclonal antibody to human epidermoid tumor in nude mice. *J. Nucl. Med.* 49(2), 295–302 (2008). [Crossref](#). [PubMed](#).
10. Wang S, Shin IS, Hancock H et al. Pulsed high intensity focused ultrasound increases penetration and therapeutic efficacy of monoclonal antibodies in murine xenograft tumors. *J. Control. Release.* 162(1), 218–224 (2012). [Crossref](#). [PubMed](#).
11. Park MJ, Kim YS, Yang J et al. Pulsed high-intensity focused ultrasound therapy enhances targeted delivery of cetuximab to colon cancer xenograft model in mice. *Ultrasound Med. Biol.* 39(2), 292–299 (2013). [Crossref](#). [PubMed](#).
12. Leighton T. In: *The Acoustic Bubble*. Academic Press, London (1994). <https://doi.org/10.1016/B978-0-12-441920-9.X5001-9>
13. Pitt WG, Hussein GA, Staples BJ. Ultrasonic drug delivery: a general review. *Expert Opin. Drug. Deliv.* 1(1), 37–56 (2004). [Crossref](#). [PubMed](#).

14. Arvanitis CD, Bazan-Peregrino M, Rifai B et al. Cavitation-enhanced extravasation for drug delivery. *Ultrasound Med. Biol.* 37(11), 1838–1852 (2011). [Crossref](#). [PubMed](#).
15. Chen H, Kreider W, Brayman AA et al. Blood vessel deformations on microsecond time scales by ultrasonic cavitation. *Phys. Rev. Lett.* 106(3), 034301 (2011). [Crossref](#). [PubMed](#).
16. Stieger SM, Caskey CF, Adamson RH et al. Enhancement of vascular permeability with low-frequency contrast-enhanced ultrasound in the chorioallantoic membrane model. *Radiology.* 243(1), 112–121 (2007). [Crossref](#). [PubMed](#).
17. Coussios CC, Farny CH, Ter Haar G, Roy RA. Role of acoustic cavitation in the delivery and monitoring of cancer treatment by high-intensity focused ultrasound (HIFU). *Int. J. Hyperth.* 23(2), 105–120 (2007). [Crossref](#). [PubMed](#).
18. Gyongy M, Arora M, Noble JA, Coussios CC. Use of passive arrays for characterization and mapping of cavitation activity during HIFU exposure. In: *2008 IEEE Ultrasonics Symposium*, 871–874 (2008).
 - This work presented a novel algorithm for mapping cavitation in real-time during high-intensity focused ultrasound (HIFU) treatment, using a commercially available ultrasound scanning system.[Crossref](#).
19. Gyongy M, Coussios C. Passive spatial mapping of inertial cavitation during HIFU exposure. *IEEE Trans. Biomed. Eng.* 57(1), 48–56 (2010). [Crossref](#). [PubMed](#).
20. Arvanitis CD, Livingstone MS, McDannold N. Combined ultrasound and MR imaging to guide focused ultrasound therapies in the brain. *Phys. Med. Biol.* 58(14), 4749–4761 (2013). [Crossref](#). [PubMed](#).
21. Coviello C, Kozick R, Choi J et al. Passive acoustic mapping utilizing optimal beamforming in ultrasound therapy monitoring. *J. Acoust. Soc. Am.* 137(5), 2573–2585 (2015). [Crossref](#). [PubMed](#).
22. Kinoshita M, McDannold N, Jolesz FA, Hynynen K. Noninvasive localized delivery of Herceptin to the mouse brain by MRI-guided focused ultrasound-induced blood-brain barrier disruption. *Proc. Natl. Acad. Sci. USA.* 103(31), 11719–11723 (2006).
 - This study investigated delivery of the therapeutic antibody herceptin using ultrasound (US)-mediated cavitation of intravenously administered microbubbles to disrupt the blood–brain barrier. The amount of antibody delivered to the brain with and without US treatment was quantified.[Crossref](#). [PubMed](#).
23. Kinoshita M, McDannold N, Jolesz FA, Hynynen K. Targeted delivery of antibodies through the blood–brain barrier by MRI-guided focused ultrasound. *Biochem. Biophys. Res. Commun.* 340(4), 1085–1090 (2006). [Crossref](#). [PubMed](#).
24. Bush AI, Raymond SB, Treat LH et al. Ultrasound enhanced delivery of molecular imaging and therapeutic agents in Alzheimer's disease mouse models. *PLoS ONE.* 3(5), e2175 (2008). [Crossref](#). [PubMed](#).
25. Arvanitis CD, Askoxylakis V, Guo Y et al. Mechanisms of enhanced drug delivery in brain metastases with focused ultrasound-induced blood-tumor barrier disruption. *Proc. Natl. Acad. Sci. USA.* 115(37), E8717–E8726 (2018). [Crossref](#). [PubMed](#).
26. Bazan-Peregrino M, Rifai B, Carlisle RC et al. Cavitation-enhanced delivery of a replicating oncolytic adenovirus to tumors using focused ultrasound. *J. Control. Release.* 169(1–2), 40–47 (2013). [Crossref](#). [PubMed](#).

27. Carlisle R, Choi J, Bazan-Peregrino M et al. Enhanced tumor uptake and penetration of virotherapy using polymer stealthing and focused ultrasound. *J. Natl. Cancer Inst.* 105(22), 1701–1710 (2013). [Crossref](#). [PubMed](#).
28. Graham SM, Carlisle R, Choi JJ et al. Inertial cavitation to non-invasively trigger and monitor intratumoral release of drug from intravenously delivered liposomes. *J. Control. Release.* 178, 101–107 (2014). [Crossref](#). [PubMed](#).
29. Myers R, Coviello C, Erbs P et al. Polymeric cups for cavitation-mediated delivery of oncolytic vaccinia virus. *Mol. Ther.* 24(9), 1627–1633 (2016).
•• This study demonstrated increased delivery of an oncolytic vaccinia virus to xenograft tumors exposed to the US-mediated cavitation of SonoTran Particles and showed decreased tumor growth following this treatment.
[Crossref](#). [PubMed](#).
30. Thomas E, Menon JU, Owen J et al. Ultrasound-mediated cavitation enhances the delivery of an EGFR-targeting liposomal formulation designed for chemo-radionuclide therapy. *Theranostics.* 9(19), 5595–5609 (2019). [Crossref](#). [PubMed](#).
31. Dimcevski G, Kotopoulis S, Bjanes T et al. A human clinical trial using ultrasound and microbubbles to enhance gemcitabine treatment of inoperable pancreatic cancer. *J. Control. Release.* 243, 172–181 (2016). [Crossref](#). [PubMed](#).
32. Kwan JJ, Myers R, Coviello CM et al. Ultrasound-propelled nanocups for drug delivery. *Small.* 11(39), 5305–5314 (2015). [Crossref](#). [PubMed](#).
33. Kwan JJ, Graham S, Myers R et al. Ultrasound-induced inertial cavitation from gas-stabilizing nanoparticles. *Phys. Rev. E Stat. Nonlin. Soft Matter Phys.* 92(2), 23019 (2015). [Crossref](#).
34. Myers R, Grundy M, Rowe C et al. Ultrasound-mediated cavitation does not decrease the activity of small molecule, antibody or viral-based medicines. *Int. J. Nanomedicine.* 13, 337–349 (2018). [Crossref](#). [PubMed](#).
35. Mannaris C, Bau L, Grundy M et al. Microbubbles, nanodroplets and gas-stabilizing solid particles for ultrasound-mediated extravasation of unencapsulated drugs: an exposure parameter optimization study. *Ultrasound Med. Biol.* 45(4), 954–967 (2019). [Crossref](#). [PubMed](#).
36. Gray MD, Elbes D, Paverd C et al. Dual array passive acoustic mapping for cavitation imaging with enhanced 2-D resolution. *IEEE T. Ultrason. Ferr.* (2020). [Crossref](#). [PubMed](#).
37. Reed GF, Lynn F, Meade BD. Use of coefficient of variation in assessing variability of quantitative assays. *Clin. Diagn. Lab. Immunol.* 9(6), 1235–1239 (2002). [PubMed](#).
38. Bates D, Machler M, Bolker B, Walker S. Fitting linear mixed-effects models using lme4. *arXiv Prepr. arXiv1406.5823.* (2014).
39. R Core Team 2018. R: a language and environment for statistical computing. (2018). www.r-project.org/
40. Luke SG. Evaluating significance in linear mixed-effects models in R. *Behav. Res. Methods.* 49(4), 1494–1502 (2017). [Crossref](#). [PubMed](#).
41. Pinheiro J, Bates D, DebRoy S et al. nlme: linear and nonlinear mixed effects models. (2020). <https://cran.r-project.org/package=nlme>
42. Choi JJ, Carlisle RC, Coviello C et al. Non-invasive and real-time passive acoustic mapping of ultrasound-mediated drug delivery. *Phys. Med. Biol.* 59(17), 4861–4877 (2014). [Crossref](#). [PubMed](#).
43. Elbes D, Paverd C, Cleveland R, Coussios C. Sub-millimeter bistatic passive acoustic mapping. *J. Acoust. Soc. Am.* 141(5), 3550–3551 (2017). [Crossref](#).

44. Morel DR, Schwieger I, Hohn L et al. Human pharmacokinetics and safety evaluation of SonoVue, a new contrast agent for ultrasound imaging. *Invest. Radiol.* 35(1), 80 (2000). [Crossref](#). [PubMed](#).
45. Lazic SE. Why we should use simpler models if the data allow this: relevance for ANOVA designs in experimental biology. *BMC Physiol.* 8, 16 (2008). [Crossref](#). [PubMed](#).
46. Mannaris C, Averkiou MA. Investigation of microbubble response to long pulses used in ultrasound-enhanced drug delivery. *Ultrasound Med. Biol.* 38(4), 681–691 (2012). [Crossref](#). [PubMed](#).
47. Luo FR, Yang Z, Dong H et al. Correlation of pharmacokinetics with the antitumor activity of cetuximab in nude mice bearing the GEO human colon carcinoma xenograft. *Cancer Chemother. Pharmacol.* 56(5), 455–464 (2005). [Crossref](#). [PubMed](#).
48. Miyamoto R, Oda T, Hashimoto S et al. Cetuximab delivery and antitumor effects are enhanced by mild hyperthermia in a xenograft mouse model of pancreatic cancer. *Cancer Sci.* 107(4), 514–520 (2016). [Crossref](#). [PubMed](#).
49. Pastuskovas CV, Mundo EE, Williams SP et al. Effects of anti-VEGF on pharmacokinetics, biodistribution, and tumor penetration of trastuzumab in a preclinical breast cancer model. *Mol. Cancer Ther.* 11(3), 752–762 (2012). [Crossref](#). [PubMed](#).
50. Arjaans M, Munnink THO, Oosting SF et al. Bevacizumab-induced normalization of blood vessels in tumors hampers antibody uptake. *Cancer Res.* 73(11), 3347–3355 (2013). [Crossref](#). [PubMed](#).
51. Kwan JJ, Lajoinie G, De Jong N, Stride E et al. Ultrahigh-speed dynamics of micrometer-scale inertial cavitation from nanoparticles. *Phys. Rev. Appl.* 6(4), (2016). [Crossref](#). [PubMed](#).
52. Cunningham D, Humblet Y, Siena S et al. Cetuximab monotherapy and cetuximab plus irinotecan in irinotecan- refractory metastatic colorectal cancer. *N. Engl. J. Med.* 351(4), 337–345 (2004).
•• In this clinical trial, the efficacy of cetuximab as a monotherapy was shown to be inferior to that of a combination treatment (in terms of response rate and median time to progression).
[Crossref](#). [PubMed](#).
53. Van Cutsem E, Köhne CH, Hitre E et al. Cetuximab and chemotherapy as initial treatment for metastatic colorectal cancer. *N. Engl. J. Med.* 360(14), 1408–1417 (2009). [Crossref](#). [PubMed](#).
54. Karapetis CS, Khambata-Ford S, Jonker DJ et al. K-ras mutations and benefit from cetuximab in advanced colorectal cancer. *N Engl J Med.* 359(17), 1757–1765 (2008). [Crossref](#). [PubMed](#).
55. Saltz LB, Meropol NJ, Loehrer PJ, Needle MN, Kopit J, Mayer RJ. Phase II trial of cetuximab in patients with refractory colorectal cancer that expresses the epidermal growth factor receptor. *J. Clin. Oncol.* 22(7), 1201–1208 (2004). [Crossref](#). [PubMed](#).
56. Jain RK, Boucher Y, Wolmark N. Interstitial hypertension in human breast and colorectal Tumors. *Cancer Res.* 52(22), 6371–6374 (1992). [PubMed](#).
57. Boucher Y, Baxter LT, Jain RK. Interstitial pressure gradients in tissue-isolated and subcutaneous tumors: implications for therapy. *Cancer Res.* 50(15), 4478–4484 (1990). [PubMed](#).
58. Minchinton AI, Tannock IF. Drug penetration in solid tumours. *Nat. Rev. Cancer.* 6(8), 583–592 (2006). [Crossref](#). [PubMed](#).
59. Dewhirst MW, Secomb TW. Transport of drugs from blood vessels to tumour tissue. *Nat. Rev. Cancer.* 17(12), 738–750 (2017). [Crossref](#). [PubMed](#).
60. Park JS, Kim IK, Han S et al. Normalization of tumor vessels by Tie2 activation and Ang2 inhibition enhances drug delivery and produces a favorable tumor microenvironment. *Cancer Cell.* 30(6), 953–967 (2016). [Crossref](#). [PubMed](#).

61. Dickson PV, Hamner JB, Sims TL et al. Bevacizumab-induced transient remodeling of the vasculature in neuroblastoma xenografts results in improved delivery and efficacy of systemically administered chemotherapy. *Clin. Cancer Res.* 13(13) 3942–3950 (2007). [Crossref](#). [PubMed](#).
62. Chauhan VP, Stylianopoulos T, Martin JD et al. Normalization of tumour blood vessels improves the delivery of nanomedicines in a size-dependent manner. *Nat. Nanotechnol.* 7, 383–388 (2012). [Crossref](#). [PubMed](#).
63. Tailor TD, Hanna G, Yarmolenko PS et al. Effect of pazopanib on tumor microenvironment and liposome delivery. *Mol. Cancer Ther.* 9(6), 1798–1808 (2010). [Crossref](#). [PubMed](#).
64. Miller A, Nace R, Ayala-Breton CC et al. Perfusion pressure is a critical determinant of the intratumoral extravasation of oncolytic viruses. *Mol. Ther.* 24(2), 306–317 (2016). [Crossref](#). [PubMed](#).
65. Staruch RM, Hynynen K, Chopra R. Hyperthermia-mediated doxorubicin release from thermosensitive liposomes using MR-HIFU: therapeutic effect in rabbit Vx2 tumours. *Int. J. Hyperth.* 31(2), 118–133 (2015). [Crossref](#). [PubMed](#).
66. Tak WY, Lin SM, Wang Y et al. Phase III HEAT study adding lyso-thermosensitive liposomal doxorubicin to radiofrequency ablation in patients with unresectable hepatocellular carcinoma lesions. *Clin. Cancer Res.* 24(1), 73–83 (2018). [Crossref](#). [PubMed](#).
67. Lyon PC, Gray MD, Mannaris C et al. Safety and feasibility of ultrasound-triggered targeted drug delivery of doxorubicin from thermosensitive liposomes in liver tumours (TARDOX): a single-centre, open-label, phase 1 trial. *Lancet Oncol.* 19(8), 1027–1039 (2018). [Crossref](#). [PubMed](#).
68. Dou Y, Hynynen K, Allen C. To heat or not to heat: challenges with clinical translation of thermosensitive liposomes. *J. Control. Release.* 249, 63–73 (2017). [Crossref](#). [PubMed](#).